Research Article Vol. 34, No. 2 / 26 Jan 2026 / Optics Express 2714
Optics EXPRESS

Performance of low-coherence and confocal refractometry with reduced index contrast

DANIEL FRANCIS,* JONATHAN M. HALLAM, AND RALPH P. TATAM

Engineering Photonics, Cranfield University, MK43 0AL, UK
daniel.francis@cranfield.ac.uk

Abstract: This paper looks to evaluate the performance of combined low-coherence and confocal refractometry under conditions of reduced refractive index contrast. The instrument measures the refractive index and thickness of transparent objects using a fibre-based low-coherence interferometer with a line-scan spectrometer. A sample was designed that mimics the on-axis structure of the eye, consisting of a lens tube holding a pair of windows surrounded on either side by fluid chambers and sealed at the far end by a diffuse black metallic plug. Sucrose solutions with a range of concentrations were injected into the fluid chambers, providing a linear variation in refractive index of 1.3330 to 1.4416. The instrument was used to simultaneously measure both the phase and group refractive indices n_p and n_g, as well as the physical thickness t of the windows and the fluid in the chambers. Although the measurement accuracy is shown to decrease with reduced refractive index contrast, it remains better than 0.6% over all measured components for sucrose concentrations of up to 60.3%, which is close to the saturation limit.

Published by Optica Publishing Group under the terms of the Creative Commons Attribution 4.0 License. Further distribution of this work must maintain attribution to the author(s) and the published article's title, journal citation, and DOI.

1. Introduction

Combined low-coherence interferometry and confocal refractometry is an effective technique for non-contact measurement of the absolute thickness and refractive index of transparent media due to its ability to measure both components of the refractive index, the phase and group indices n_p and n_g, as well as the physical thickness t [1–3]. This is in contrast to low-coherence interferometry alone which can be used to measure n_g and the optical thickness [4]. It is also able to perform these measurements on samples that are much larger than is possible with conventional low-coherence interferometry, which is limited to sample thicknesses that are less than the Rayleigh range of the focusing optics. Swept-source [5] or frequency domain [6] techniques can provide a simplified solution that allows faster measurements with better accuracy and stability, but at the cost of the ability to measure n_p. Early in its development, measurements tended to focus on individual glass plates; since then however, more complex and varied applications have appeared. Applications that have been published using this and closely related techniques include liquids [7], GRIN (gradient-index) materials [8], birefringent materials [9], contact lenses [10], compound optics [11], and plastic materials [12]. These measurements are typically made with the sample in air, where the refractive index differences between the interfaces is high. As an example, the refractive indices of borosilicate crown glass and air are approximately 1.5 and 1.0 respectively, which corresponds to a reflectivity of 4% for light at normal incidence. As the refractive index contrast decreases, the reflectivity of the interfaces is reduced, and accurate measurements become more challenging.

One application that is of particular interest is the measurement of the refractive index and thickness of the optical components within the eye. These include the cornea, eye lens, and aqueous and vitreous humours. The refractive index of the humours is typically quoted as being at around 1.336 (@589 nm) [13] and there is only a small amount of variation between

#582088 https://doi.org/10.1364/OE.582088
Journal © 2026 Received 17 Oct 2025; revised 3 Dec 2025; accepted 3 Dec 2025; published 21 Jan 2026

Optics EXPRESS

individuals. The refractive index of the cornea is traditionally quoted as around 1.376, although more recent research based on *in-vivo* corneal refractometry suggests a much higher mean value at around 1.425 [14]. However, there is significant variation in the refractive indices between individuals [15]. There is also a significant variation in the refractive index of the eye lens, with individual variation as well as variation with age. Uhlhorn *et al* [16] used optical coherence tomography (OCT) [17] to measure the refractive index of 40 excised cadaverous lenses of an age range from 6–82 and found indices ranging from 1.402–1.416 (@589 nm). For low-coherence and confocal refractometry to be effective for measuring refractive index and thickness of the elements within the eye, it should be capable of accurately measuring when the refractive index difference between interfaces is 0.07 or less. This corresponds to a reflectivity of approximately 0.065% and is ~60 times lower than the reflectivity at the glass/air interface mentioned above.

The aim of the work presented here is to establish how much the reduction in refractive index contrast affects the accuracy of refractive index and thickness measurements made using low-coherence and confocal refractometry. To achieve this, a sample that mimics the on-axis, depth-sectioned structure of the eye was developed using a pair of borosilicate glass windows sealed within a lens tube. Apertures drilled into the walls of the tube allowed sucrose solutions with concentrations ranging from 0–60.3%, corresponding to refractive indices from 1.3330 to 1.4416, to be injected into the cavities between the windows. These refractive indices were measured independently with an Abbe refractometer at 589 nm. With the highest concentration solution, the difference in refractive index between the solution and the glass was <0.08 which is very close to the target refractive index difference found within the eye. The refractive index and thickness of both the windows and the fluid-filled chambers are measured with each solution occupying the sample in turn. In addition to the challenges presented by the reduced refractive index contrast, there are other difficulties including the wide dynamic range required due to the higher reflectivity of the air/glass interface at the front of the sample relative to the others and the diffuse reflection from the metallic plug located at the rear of the sample, and these are discussed in more detail in Section 3 of the paper.

2. Interferometer configuration and measurement principles

A schematic of the interferometer used in this work is shown in Fig. 1 along with a photograph of the corresponding components. The calibration and mode of operation of the interferometer is described in more detail in [3] and [18] and summarised here. The source is a 50 nm bandwidth (FWHM) super-luminescent diode (SLD) centred at 840 nm with an optical power of 10 mW, which is part of a Superlum M-T-850-HP-I Broadlighter system. This source within the system was chosen because, of the three available, it best matches the bandwidth and spectral range of the spectrometer. Light from the source is divided into two paths using a broadband coupler (Thorlabs TW850R2A2) which has 100 nm bandwidth centred at 850 nm. A pair of linear translation stages (Physik Instrumente V408) are used to mount the test object in the sample beam path, and a plane mirror and focusing lens in the reference beam path. The stages have a maximum travel of 50 mm, maximum velocity of 500 mm s^{-1}, and minimum incremental motion of 20 nm. The spectrometer (Bayspec OCT spectrograph @850) has a bandwidth of 50 nm and features a CMOS line-scan camera (Basler spL4096-140) which has a 12-bit 4,096-pixel array with a maximum single line acquisition rate of 70 kHz. Note that the low-coherence measurement is made in the time-domain however, the spectrometer is necessary to make a dispersion measurement which is described below. Light in the sample arm is collimated and focused using a pair of off-axis parabolic (OAP) mirrors (25.4 mm and 33 mm reflected focal lengths respectively). The use of OAPs over transmissive optics in the sample arm has been shown to significantly improve measurement accuracy due to the reduced impact of aberrations [19]. The shutter in the reference arm is used to block the higher intensity reference reflection

Optics EXPRESS

when making the confocal measurements and is controlled using an analogue output module housed in a compact chassis (National Instruments NI-9263 and NI cDAQ-9174 respectively).

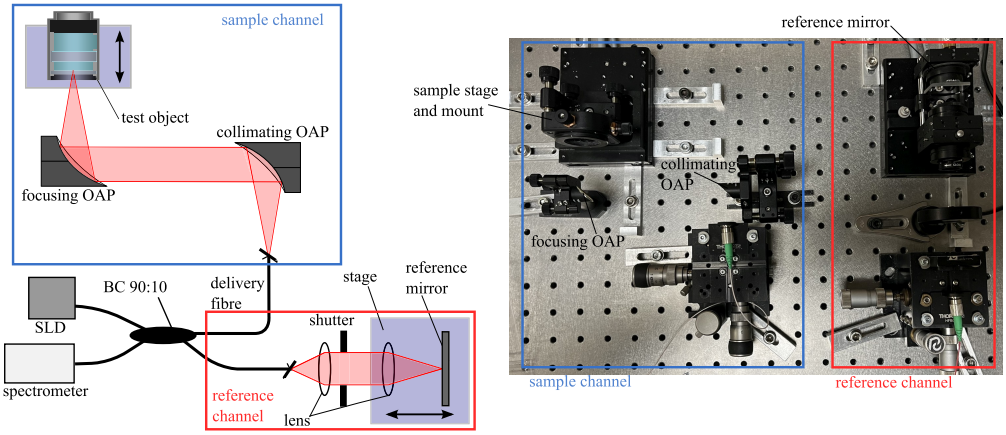


Fig. 1. Schematic showing the configuration of the interferometer. SLD - super-luminescent diode; BC - broadband coupler; OAP - off-axis parabolic mirror. The light blue shading shows the translation stages and indicates the components that are mounted on them. The photograph shows the corresponding components and how they are arranged in the sample and reference channels. The spacing of the holes in the optical bench is 2.5 cm.

When a sample is scanned linearly such that the beam is incident on each of its interfaces sequentially, light is reflected along the return path to the fibre. The 4.4 μm diameter fibre core acts as the confocal aperture in this system. A series of peaks are observed in the integrated signal of the spectrometer and, for a single element window with two interfaces, this is a pair of peaks that are separated by [20]

$$\Delta z = t \times \frac{\sqrt{(1 - NA^2)}}{\sqrt{(n_\mathrm{p} - NA^2)}} \approx \frac{t}{n_\mathrm{p}} \tag{1}$$

where NA is the numerical aperture of the focusing optics in the sample arm, which for this system is 0.093. An example of the confocal peaks acquired for a window with a thickness t = 2.161 mm are shown in Fig. 2(a) and these have a separation Δz = 1.425 mm. The low-coherence measurement is made by scanning the reference stage through the point of phase matching with the sample beam focused on each interface in turn. This is required because, at >2 mm, the window thickness is much greater than the Rayleigh range of the focusing optic. An example of the low-coherence fringe envelopes acquired using the same sample is shown in Fig. 2(b). The envelope separation, ΔD, plus the confocal term Δz calculated previously, is related to the thickness and the group refractive index by [20]

$$\Delta l = \Delta D + \Delta z = t \times n_\mathrm{g} \tag{2}$$

In this example ΔD = 1.868 mm, resulting in a distance Δl = 3.293 mm. The fluctuation in the signal seen between the two fringe sets, after the reference stage has translated 1 mm, is due to the motion of the sample translation stage as it moves from one surface to the other. Accurate measurement of ΔD requires the demodulation of the envelope of each of sets of interference fringes. There are several methods of achieving this [21] and the technique used in this work is based on the Hilbert transform [22].

Optics EXPRESS

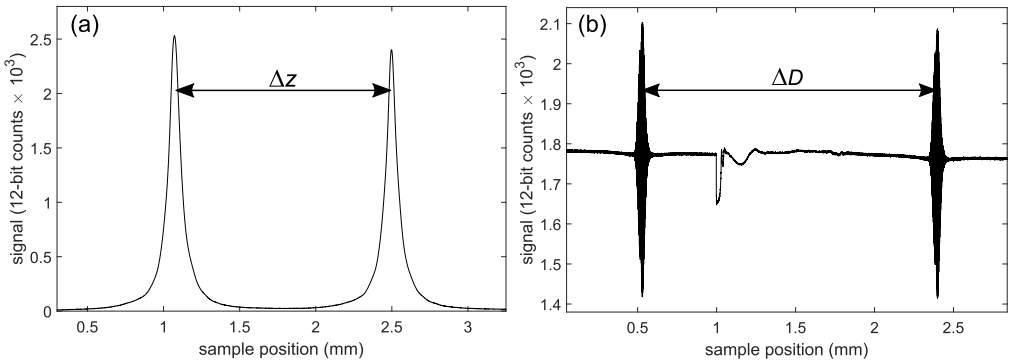


Fig. 2. Plots showing (a) the confocal peaks separated by Δz = 1.425 mm, and (b), the low-coherence fringe envelopes separated by ΔD = 1.868 mm. These measurements were obtained using a 2.161 mm thick BK7 glass window.

The group index is dependent on the chromatic dispersion

$$n_g(\nu) = n_p(\nu) + \nu \frac{dn_p(\nu)}{d\nu} \tag{3}$$

where ν is the optical frequency. Therefore, n_p and thus Δz are functions of frequency. In the case that $NA^2 \ll 1$, the approximation given in Eq. (1) can be used. Substituting this and equation Eq. (2) into Eq. (3) yields

$$t^2 = \frac{\Delta l \Delta z}{1 - \frac{\nu}{\Delta z}\frac{d\Delta z}{d\nu}} \tag{4}$$

where $d\Delta z/d\nu$ is the dispersion of the confocal parameter. In general, the mathematical approximation given in Eq. (1) and used to derive Eq. (4) cannot be applied without introducing significant measurement error and a more complex polynomial solution must be used as given by [2]

$$At^2 + Bt^4 + Ct^6 + D = 0 \tag{5}$$

where

$$\begin{aligned} A &= \frac{\left(n_{air}^2 - NA^2\right)^2}{\Delta z^4} + \nu^2 \frac{\left(n_{air}^2 - NA^2\right)^2}{\Delta z^6}\left(\frac{d\Delta z}{d\nu}\right)^2 - 2\nu \frac{\left(n_{air}^2 - NA^2\right)^2}{\Delta z^5}\frac{d\Delta z}{d\nu} \\ B &= 2\frac{\left(n_{air}^2 - NA^2\right)}{\Delta z^2}NA^2 - 2NA^2\nu\frac{\left(n_{air}^2 - NA^2\right)}{\Delta z^3}\frac{d\Delta z}{d\nu} \\ C &= NA^4 - \frac{\Delta l^2}{\Delta z^2} - \left(n_{air}^2 - NA^2\right) \\ D &= -\Delta l^2 NA^2 \end{aligned} \tag{6}$$

Once t has been obtained using Eq. (6), n_p and n_g can be calculated using Eq. (1) and Eq. (2). Equation (6) is used for all the refractive index and thickness calculations made in Section 4. To calculate the dispersion term $d\Delta z/d\nu$, each of the spectra acquired during the confocal scan is divided into a series of wavelength bins that are approximately 1.5 nm wide. The signal within each wavelength bin is integrated to generate confocal peaks, and the separation Δz is calculated for each. These are plotted against wavelength to generate a dispersion curve and the term $d\Delta z/d\nu$ can be computed from the gradient. Examples of dispersion curves are shown in Fig. 7 in Section 3. For the example described above and illustrated in Fig. 2, using a measured value of $d\Delta z/d\nu = 4.618\times10^{-17}$ ms results in a calculated thickness t = 2.156 mm and refractive indices n_p = 1.501 and n_g = 1.527.

Optics EXPRESS

3. Sample design and measurement procedure

This section describes the construction of the model eye test object and the issues surrounding measurements made using it. The sample, illustrated in Fig. 3, consists of a 25.4 mm diameter lens tube with a pair of internally mounted windows with a black aluminium plug placed at the rear of the tube. Each of the components is sealed in place with a water-resistant epoxy and a pair of holes of approximately 1 mm diameter drilled into the walls of the tube to allow fluid to be injected into the fluid chambers that separate the windows. The two windows W_1 and W_2 are constructed from BK7 crown glass and have nominal thicknesses of 1 mm and 3 mm respectively and represent the cornea and eye lens in terms of their relative position and thickness. The fluid chambers F_1 and F_2 are approximately 3 mm and 6 mm wide respectively and represent the aqueous and vitreous humours, with the outer surface of the plug at the rear of the sample corresponding to the outer surface of retina.

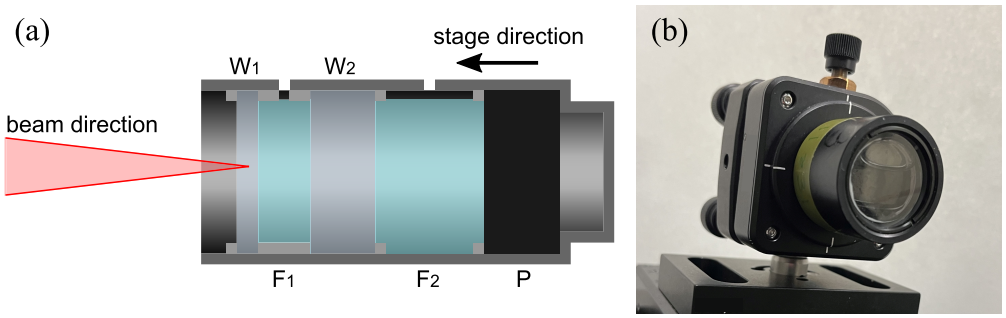


Fig. 3. (a) A schematic of the model eye sample. W_1 and W_2 are the two windows, F_1 and F_2 are the two fluid chambers, and P is the black aluminium plug. The direction of stage motion relative to the beam direction when making the measurements is indicated. (b) A photograph showing the sample in a 5-axis kinematic mount. Note that fluid chamber F_1 can be seen to be ~3/4 full here. The lens tube is 25.4 mm in diameter and in overall length.

Confocal peaks acquired during a scan through the fluid filled test sample are shown in Fig. 4. The fluid in this example is a sucrose solution with a concentration of 30.4% which has a refractive index of 1.3817 (@589 nm). Preparation of the sucrose solutions is described in Section 4. The magnitude of the first confocal peak (at ~2 mm) is much greater than that of subsequent peaks because the refractive index difference of the media either side of the air-glass interface is much greater (~1.5 – 1) than that of the glass-fluid interfaces (~1.5 – ~1.38). In contrast to this, the confocal peaks obtained with the single window in air shown in Fig. 2(a) have a much smaller difference in magnitude. The need to be able to get a well-resolved confocal peak from this front interface, without saturating the spectrometer signal prevents simply increasing the optical power to deal with the reduced reflectivity from the low refractive index contrast at the other interfaces. An example of the low-coherence fringe bursts acquired by bringing the focus to each interface in turn and scanning the reference mirror is shown in Fig. 4(b). The reference stage velocity over the course of the measurement is not constant, in this case being at 2 mm s^{-1} during the interface scan and 20 mm s^{-1} in between. This can be seen in the difference in data-point density throughout the plot. The difference in the background signal level for the three central envelopes is due to the difference in the magnitude of the interface reflection.

The confocal peak associated with the reflection from the plug, seen at a stage position of ~11 mm in Fig. 4(a), is not as well defined as the other peaks that are due to reflections from either air-glass or water-glass interfaces, with several side features existing either side of the main peak. This peak is shown plotted over a shorter distance scale in Fig. 5(a). The shape of this peak is very susceptible to alignment, with small adjustments of the orientation of the sample mount

Optics EXPRESS

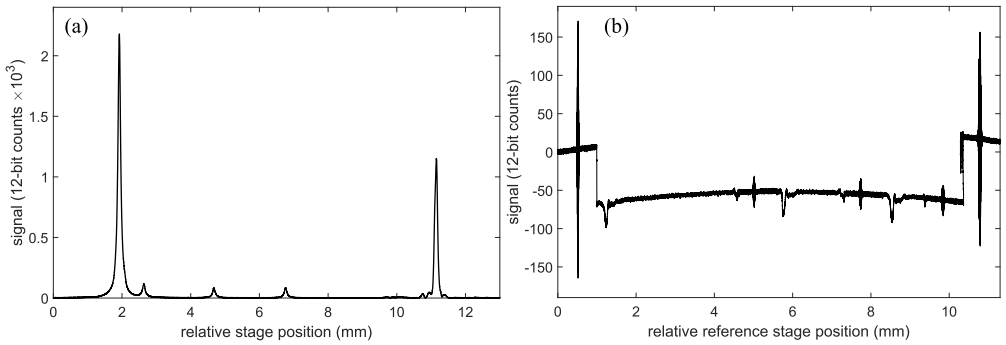


Fig. 4. Plots showing (a) the confocal peaks and (b) the low-coherence fringe envelopes acquired by scanning through the fluid filled sample. This data was acquired with a sucrose solution of 30.4% present within both the fluid chambers.

or focusing optic causing significant changes in the peak shape. To illustrate this, Fig. 5(b – d) shows three more confocal peaks that were acquired from the plug surface with small adjustments to the sample orientation between each. In each case, the other peaks from the other sample interfaces remained well-defined, with little or no change in the peak magnitude. Whilst the peak in Fig. 5(d) looks well-defined, in this case the reflection from the plug was sufficiently high to saturate the sensor of the line-scan camera and therefore its centre location is unreliable.

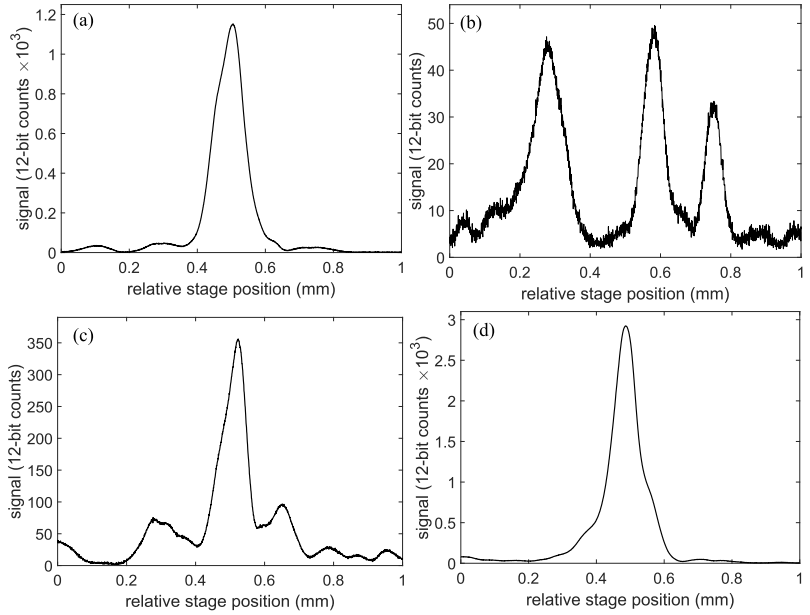


Fig. 5. Confocal peaks associated with the reflection from the surface of the metallic plug P at the rear of the sample. (a) is taken from the same dataset as Fig. 4(a). The peaks in (b), (c), and (d) were acquired with slightly different alignments of the sample beam that maintained well-defined peaks for each of the other reflections.

The cause of this high level of variability in the peak shape can be investigated further by looking at raw spectra acquired from each of the peaks. Figure 6 shows spectra taken with the beam focused on the rear interface of W_2 (a) and on the plug surface (b). The shape of the

Optics EXPRESS

spectrum in Fig. 6(a) follows the spectral intensity distribution of the source and is consistent for the other three interfaces in the sample. The spectrum acquired from the plug surface shows a significant amplitude modulation that is not seen in any of the peaks from the other interfaces. With small changes in the sample's orientation relative to the beam the period of the fringe pattern does not change but is highly variable in phase and amplitude. The mean free spectral range of the fringe pattern in Fig. 6(b) is 13.6 nm which corresponds to an associated cavity length of 39 μm. This suggests that the fringe pattern is caused by the speckle effect [23] which is due to the diffuse reflection from the optically rough surface of the plug which would have features on the scale of this cavity, and accounts for the highly variable nature of the confocal peak.

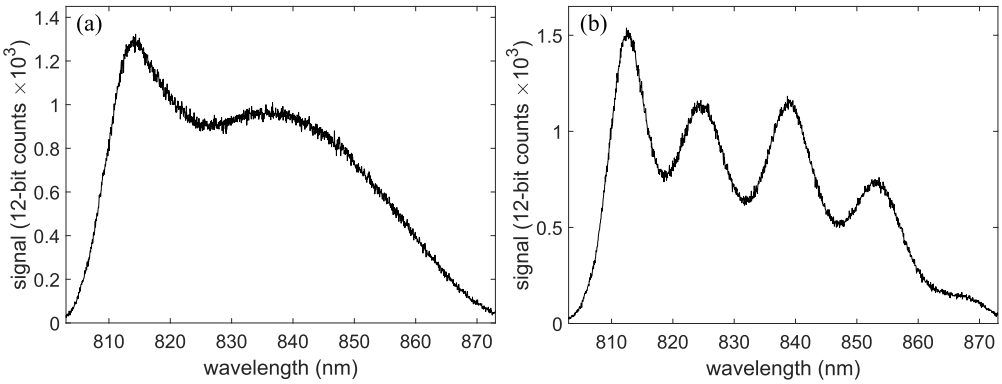


Fig. 6. Raw spectra acquired with the beam focused on (a) the glass-fluid interface at the rear of the window W_2 and (b) from the plug. These space between these two interfaces forms the fluid chamber F_2 in Fig. 3 which contains deionized water in this example.

Spectrometer-based dispersion measurements made for each of the sample elements $W_{1,2}$ and $F_{1,2}$ are shown in Fig. 7. The gradient of these data is used to calculate the $d\Delta z/d\nu$ term used in Eq. (6). The data from W_1 (a) is noisier than F_1 (b) and W_2 (c) because this window is thinner than the others meaning that there is less dispersion across the spectral range, and here the change in Δz over the full range is only ~3 μm compared to ~10-12 μm for F_1 and W_2, which can make it very challenging to derive the true gradient. Data-points at the extremes of the spectral range are often outliers due to the lower signal at the edges of the spectrum and it can be helpful to omit these when determining the gradient. The dispersion gradient from F_2 (d) is completely obscured by the fringe pattern originating from the plug surface reflection. The refractive index of the fluid and the thickness of the chamber F_2 can be calculated by assuming the dispersion is the same as that of the fluid in the first chamber.

4. Refractive index and thickness measurements

Sucrose (Sigma-Aldrich >99.5% purity) was used as means of generating a series of solutions with approximately linearly varying refractive index. The concentration of the solutions ranged from 0% (pure deionized water) to 60.3%. The saturation limit of sucrose in water at 20°C is approximately 2 kg/l or a concentration of ~66.6%. Deionized water and sucrose were weighed on a sub-milligram scale and mixed into solution using a magnetic stirrer. The refractive index of each solution was measured using an Anton Parr Abbemat 200 refractometer which provides accurate measurements of the refractive index of fluids at the sodium D2-line wavelength of 589.0 nm. The measured refractive index values can be used to determine the concentration of sucrose based on values presented in the CRC Handbook of Chemistry and Physics [24] and measurements of the laboratory ambient temperature. Table. 1 shows a summary of the

Optics EXPRESS

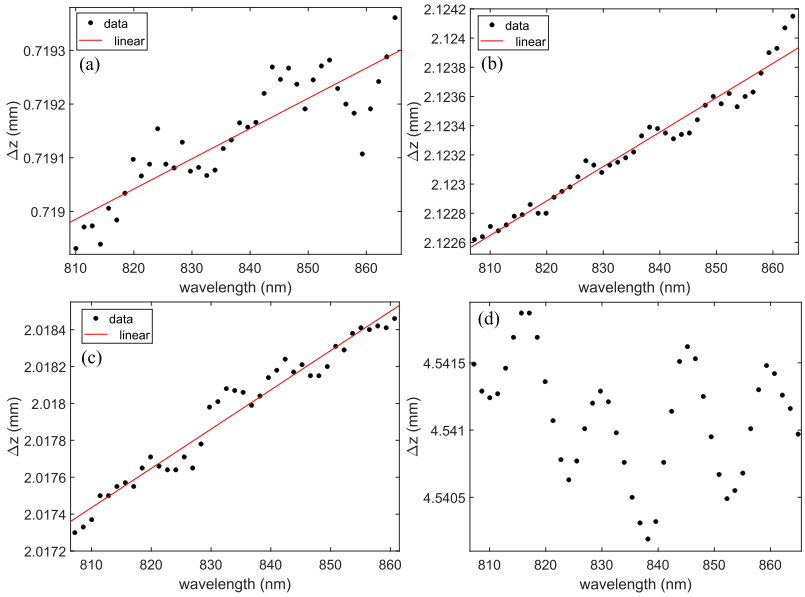


Fig. 7. Dispersion measurements made from (a) W_1, (b) F_1, (c) W_2, and (d) F_2. Linear fits to the data are also shown in (a – c). A dispersion gradient in (d) cannot be obtained due to the fringe pattern associated with the plug reflection. The measurements were made with deionized water in the fluid chambers.

Abbe measured refractive indices of the sucrose solutions and their temperature corrected concentrations. The wide variation in temperatures in Table. 1 is because the solutions were prepared as and when they were needed which may have been several days apart.

Table 1. Summary of the Abbe measured refractive indices and corresponding concentrations of the sucrose solutions used in this work. A correction to the concentration needs to be applied based on the temperature of the environment [24]

Solution	Measured RI (@589 nm)	Concentration	Ambient Temp	T Corrected Concentration
0	1.3330	0%	25.1°C	0%
1	1.3469	9.3%	21.7°C	9.4%
2	1.3644	20.3%	20.3°C	20.3%
3	1.3817	30.3%	21.7°C	30.4%
4	1.4002	40.2%	23.4°C	40.4%
5	1.4203	50.1%	23.0°C	50.3%
6	1.4416	59.9%	25.0°C	60.3%

Refractive index and thickness measurements of each of the elements within the sample were made using each of the sucrose solutions. Each of the measurements sets was made within the course of a day, to limit the impact of evaporation changing the concentration during each measurement set. To verify the impact of the stage scanning speed on measurement accuracy three speed regimes were utilized, which are summarized in Table. 2, along with the measurement durations that were achieved with them. The paths followed by the translation stages during a typical measurement, under conditions of speed regime 1, are shown in Fig. 8. Speed regime 3 corresponds to the fastest stage velocities that continued to yield uncertainties of better than 0.1%

Optics EXPRESS

across all three measured components in our previous publication [18]. After initializing the camera and stages, the confocal scan is performed in a single motion of the sample stage. Then, after reinitializing the line-scan camera to adjust the exposure time, the low-coherence scans are performed with the sample beam focused on each interface in turn.

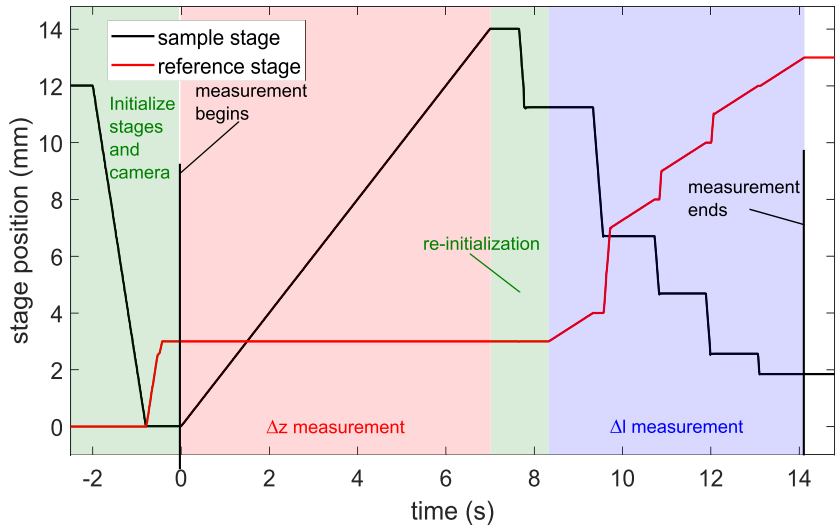


Fig. 8. Plot showing the paths of the two translation stages, sample stage 1 (black) and reference stage 2 (red) over the course of a measurement of the sample in Fig. 3. The confocal scan (Δz measurement) is highlighted in red and runs from 0 – 7 s, and the low-coherence scans (Δl measurement) is highlighted in blue and runs from 8.4 – 14.1 s. The stage velocities correspond to speed regime 1 in Table. 2.

Table 2. Summary of the stage velocities and the total measurement time for each of the speed regimes used for refractive index and thickness measurement

Speed regime	Stage 1 velocity	Stage 2 velocity (scan)	Measurement time
1	2 mm s^{-1}	1 mm s^{-1}	14.1 s
2	5 mm s^{-1}	2 mm s^{-1}	7.4 s
3	10 mm s^{-1}	3 mm s^{-1}	5.2 s

The measurements were repeated six times for each speed regime using each of the sucrose solutions. Table. 3 summarises the refractive index and thickness measurements made using deionized water (0% sucrose solution) under the conditions of speed regime 2. The measurements were repeated six times with the mean value being given in the table along with its standard deviation. The percentage errors for the refractive index measurements were calculated from the difference between the measured value and the reference value at 840 nm. These reference values [25] were obtained from the literature for BK7 [26] and deionized water [27]. The refractive index for water was calculated at three different temperatures in [27], so the value for 24°C was used here as it is closest to the measured ambient temperature of 25.1°. The reference thickness values for the two windows were measured using a precision micrometer gauge (0.1 µm resolution Mitutoyo MDH). The micrometer measurements were also made six times and thus have a standard deviation associated with them, given in the 'Thickness' column in Table. 3. The refractive index and thickness measurements for all the other sucrose solutions and speed regimes are provided in the supplementary material document.

Optics EXPRESS

Table 3. Summary of refractive index and thickness measurements repeated six times with pure deionized water in the fluid chambers of the sample. Objects W_1 and W_2 are the BK7 windows and F_1 and F_2 are the fluid chambers. Measurements were made under the conditions of speed regime 2. Reference index values for BK7 [26] and H_2O [27] are provided in the headings.

	Phase index (n_p) (BK7 = 1.5100, H_2O = 1.3276)			Group index (n_g) (BK7 = 1.5252, H_2O = 1.3412)			Thickness (t) (mm) (W_1 = 1.0884, SD = 0.00055) (W_2 = 3.1524, SD = 0.00105)		
Obj	Meas	St dev	Err(%)	Meas	St dev	Err(%)	Meas	St dev	Err(%)
W_1	1.5104	0.00259	0.0265	1.5253	0.00275	0.0066	1.0864	0.00093	0.1868
F_1	1.3287	0.00116	0.0703	1.3404	0.00126	0.0857	2.8106	0.00265	NA
W_2	1.5097	0.00095	0.0177	1.5243	0.00117	0.0579	3.1494	0.00209	0.0946
F_2	1.3313	0.00247	0.1243	1.3399	0.00257	0.1230	6.0041	0.01142	NA

Refractive index measurements for the pairs of windows and fluid chambers at each concentration step are shown in Fig. 9, with data in (a) being acquired under the conditions of speed regime 1 and (b) under the conditions of speed regime 3. The data that was used to produce the plots is provided in the supplementary material document. The vertical grey banding separates the plots into distinct regions corresponding to each sucrose concentration, with the data-points being placed in the white regions. The position of the data-point, from left-to-right, within each white band corresponds to the position of the object within the sample, e.g. data from window W_1 is located to the left of each band, and data from fluid chamber F_2 is located to the right of each band. The refractive indices of the two windows are plotted in blue for n_p and green for n_g with the refractive index value plotted on the left y-axis, and for the two fluid chambers these are plotted in red for n_p and purple for n_g with the values plotted on the right y-axis. Each data-point is the mean of six measurements and the magnitude of the error bars corresponds to the standard deviation of those measurements. The black horizontal lines represent the reference refractive index values for BK7 and water that are given in the headings of Table. 3. There are no reference values for the sucrose solutions, as the independent measurements made using the Abbe were limited to a single wavelength, 589 nm. Sellmeier coefficients for sucrose solutions at different concentrations have been reported [28], however the refractive index values published are far enough from the measurements that we made with our Abbe and those reported in the Handbook of Chemistry and Physics [24] that they are considered an unreliable source for a reference (e.g. the measured values for 30% sucrose concentration differ by ~0.7%).

The accuracy of the refractive index measurements of the two glass windows is generally good at the slower stage velocities, with data-points being close to the reference values and having small error bars, although these are larger for W_1. This is due to W_1 being thinner and therefore more difficult to determine the dispersion gradient, as discussed previously. The faster stage velocities particularly impact the accuracy of the n_g measurements whilst there is also an increase in the size of the error bars at higher sucrose concentrations. The error bars of the fluid chamber refractive index measurements are larger for F_2 than F_1 (apart from at 60.3% sucrose concentration in Fig. 2(b)) which is expected given the issues related to the plug measurement discussed in the previous section. The refractive index values of F_2 match those of F_1 more closely for some sucrose solutions than others although this does not appear to worsen due to either increased sucrose concentration or stage velocity, and this mismatch is generally within the error bars of the F_2 measurements, so it is within the experimental error of this more challenging measurement. The plot in Fig. 10 shows the refractive index measurements for the fluid chamber F_1 and the linear fit to the data for each of the speed regimes. They each show good linearity with R^2 values greater than 0.995 and means of residuals that are close to zero ($<10^{-16}$).

Optics EXPRESS

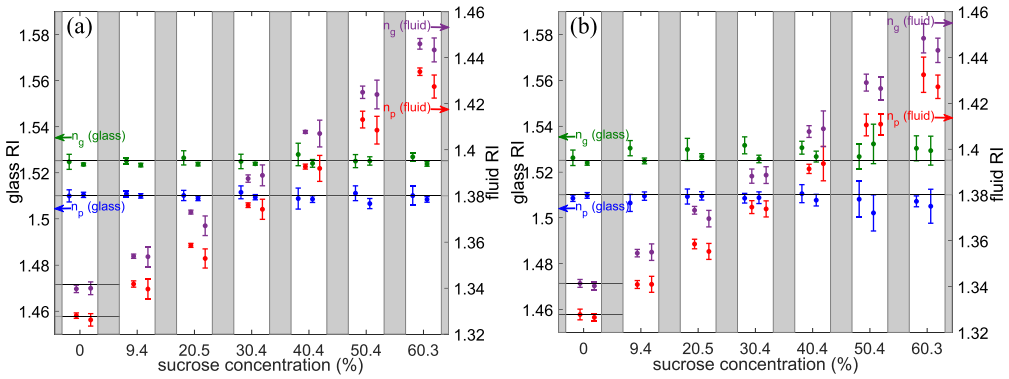


Fig. 9. Refractive index measurements made with various sucrose solutions present in the fluid chambers under the conditions of (a) speed regime 1 and (b) speed regime 3 (see Table. 2). The phase and group indices of the glass windows W_1 and W_2 are plotted in blue and green on the left *y*-axis, and of the fluid chambers F_2 and F_2 in red and purple on the right *y*-axis respectively. Black horizontal lines represent the reference index values for BK7 and water (0% sucrose) at 840 nm. The grey banding serves to divide the plot in separate regions corresponding to the different sucrose concentrations.

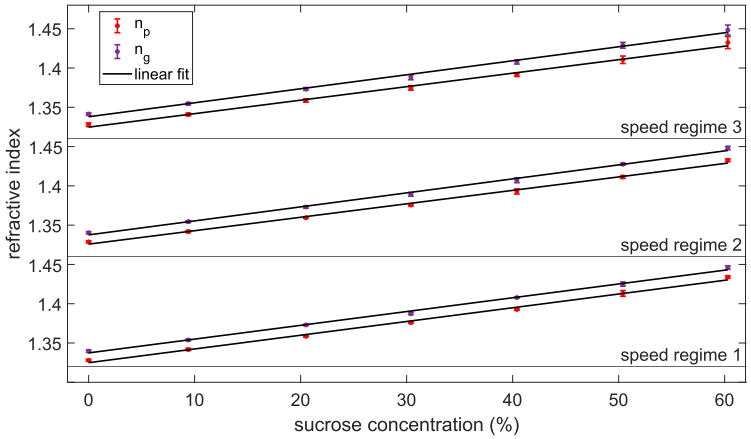


Fig. 10. Refractive index measurements for fluid chamber F_1 for each of the speed regimes with the linear fit to each dataset.

Thickness measurements made with the various sucrose solutions under the conditions of speed regimes 1 and 3 are shown in Fig. 11(a) and (b) respectively. In these plots, the *y*-axis is divided into four separate regions covering each of the four elements, which are in order of increasing thickness going up the axis (W_1, F_1, W_2, and then F_2). The vertical grey bands serve to separate the data into distinct regions for each sucrose solution with the spatial location of the data-point within each white band again corresponding to its position within the sample, with the window thickness plotted in blue and the fluid chamber thicknesses in red. The solid black horizontal lines within the glass window thickness measurements are the reference values made with the Vernier gauge (given in Table. 3), and the dashed horizontal lines in the fluid chamber measurements are the mean of all values within that row. The error bars in the second fluid chamber F_2 (top row) measurements are much larger than the others therefore the *y*-axis range is greater than the others to show them clearly. The accuracy and repeatability of measurements is better at lower stage velocities, particularly for the window W_2, and for the most part, at lower

Optics EXPRESS

sucrose concentrations, which is as expected. There is an underestimate in the thicknesses of the windows, likely caused by a slight misalignment of the illumination beam relative to the sample surfaces, which becomes more pronounced at higher stage velocities and higher sucrose concentrations.

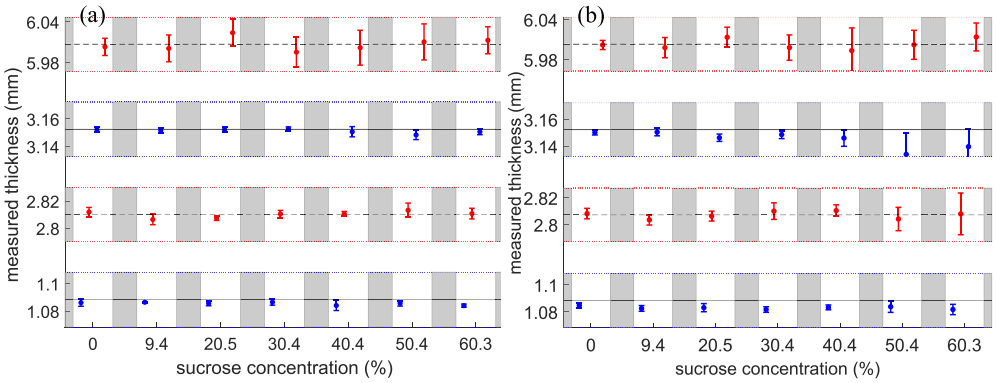


Fig. 11. Thickness measurements made with various sucrose solutions under the conditions of (a) speed regime 1 and (b) speed regime 3 (see Table. 2). The samples are plotted in order (going up the y-axis) of increasing thickness (W_1, F_1, W_2, and then F_2). Window and fluid chamber thickness are plotted in blue and red respectively, with the solid black horizontal lines representing the reference measurement made with a Vernier gauge and the dashed horizontal lines representing the mean value of the row.

The lowest percentage error of all the measurements was 0.5199% for refractive index and 0.5874% for thickness and these were both for window W_2 made using 50.4% sucrose solution under speed regime 3. One of the main reasons that the accuracy is lower here is that it is much more difficult to accurately determine the dispersion gradient. Figure 12(a) shows an example of a dispersion measurement made on W_2 under these conditions with a linear fit to the data highlighting the difficulty in accurately determining the gradient when compared with the dispersion measurements made using deionized water shown in Fig. 7. The accuracy of the thickness measurements on W_1 using 60.3% sucrose solution under speed regime 3 also proved difficult and a dispersion measurement on W_1 is shown in Fig. 12(b).

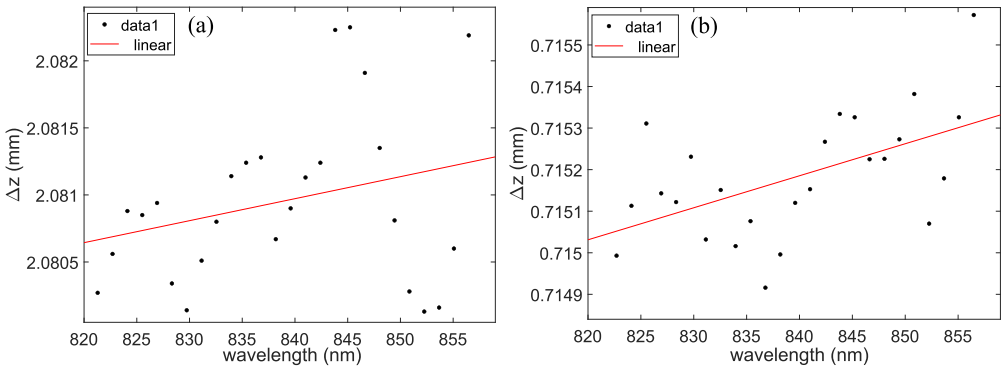


Fig. 12. Dispersion measurements made on (a) window W_2 with sucrose concentration of 50.4% and (b) window W_1 with sucrose concentration of 60.3% under speed regime 3 with linear fits to the data.

Optics EXPRESS

An alternative to measuring the dispersion of Δz across the spectrometer is to calculate $d\Delta z/d\nu$ using a reference value of dispersion $dn/d\lambda$ and Eq. (1). For BK7 glass at 840 nm, $dn/d\lambda$ = -0.018085 μm^{-1}) [25], [26]. The refractive index and thickness measurements made for W_1 and W_2 under the conditions discussed using the spectrometer-based dispersion measurement are summarized in the upper half of Table. 4 and using the reference calculation in the lower half. The same confocal and low-coherence measurement data was used to calculate both sets of values. There is a significant improvement in the accuracy when using the dispersion calculation with percentage errors in refractive index measurements better than 0.1% and better than 0.4% for thickness measurements, and there is also a reduction in the standard deviations of the measurements.

Table 4. Refractive index and thickness measurements made six times for W_1 with sucrose concentration of 60.3% and for W_2 with sucrose concentration of 50.4% under speed regime 3. The values are obtained based on the spectrometer-based dispersion measurement of $d\Delta z/d\nu$ (upper half of table) and a calculation of $d\Delta z/d\nu$ made using the reference dispersion value for BK7 glass ($dn/d\lambda$ = -0.018085 μm^{-1}) and Eq. (1) (lower half of table). *BK7 [26]. Thickness reference values are mean of six independent Vernier measurements with associated standard deviations

	Phase index (n_p) (BK7* = 1.5100)			Group index (n_g) (BK7* = 1.5252)			Thickness (t) (mm) (W_1 = 1.0884, SD = 0.00055) (W_2 = 3.1524, SD = 0.00105)		
Obj	Meas	St dev	Err(%)	Meas	St dev	Err(%)	Meas	St dev	Err(%)
W_1 (60.3%)	1.5072	0.00216	0.1854	1.5303	0.00498	0.3366	1.0824	0.00243	0.5513
W_2 (50.4%)	1.5022	0.00720	0.5199	1.5323	0.00786	0.4622	3.1339	0.01480	0.5874
Obj	**Meas**	**St dev**	**Err(%)**	**Meas**	**St dev**	**Err(%)**	**Meas**	**St dev**	**Err(%)**
W_1 (60.3%)	1.5106	0.00177	0.0408	1.5266	0.00146	0.0907	1.0842	0.00124	0.3859
W_2 (50.4%)	1.5093	0.00094	0.0453	1.5250	0.00094	0.0131	3.1485	0.00223	0.1232

5. Discussion and conclusions

This paper has investigated the influence of the refractive index contrast on the accuracy and repeatability of refractive index and thickness measurements using low-coherence and confocal refractometry with broadband dispersion measurements. This has been achieved using sucrose solutions with linearly varying refractive indices from 1.3330 to 1.4416 (@589 nm) contained with a test sample comprising a pair of borosilicate glass windows and sealed with a black aluminium plug. Accurate measurements were made using all solutions which corresponds to a refractive index difference of ~0.08, which is close to the refractive index differences between the cornea/lens and humours within the eye. Measurements made with each solution were performed using three different speed regimes corresponding to measurement durations ranging from 14.1 – 5.2 s. Measurement speed is a particularly important consideration for *in – vivo* eye measurements.

Good refractive index and thickness measurements were made using all the sucrose solutions however, as the refractive index contrast reduces and the stage velocity increases, the accuracy of the measurements decreases. This is due to reduced resolution of the confocal peaks in the spectrometer signal and is particularly apparent in the dispersion measurement which relies on the detection in very small (sub-micron) variations in the confocal parameter Δz. The percentage error across all measurements here is better than 0.6%, compared to the better than 0.1% for measurements in air (high refractive index contrast) for similar stage velocities that we published previously [18]. The accuracy can be improved by calculating the dispersion of Δz using known or approximate values of $dn/d\lambda$ Consequently, in situations where the noise on the dispersion measurements is large, the uncertainty introduced from an inaccurate determination of the

Optics EXPRESS

gradient may be greater than the uncertainty introduced by approximating the value of $\mathrm{d}n/\mathrm{d}\lambda$. Cauchy dispersion coefficients of the ocular media of the eye are provided in a publication by Atchison and Smith [29], which could be used to get a good general estimate of $\mathrm{d}\Delta z/\mathrm{d}\nu$ for each of the individual components within the eye.

Measurement accuracy could be further improved by incorporating faster spectral acquisition and digitization which would allow better resolution of the confocal peaks. Better dynamic range in the line-scan sensor would also help deal with the large difference in reflectivity between the front surface and subsequent interfaces within the sample. If online measurement of the dispersion is not required, because $\mathrm{d}\Delta z/\mathrm{d}\nu$ is being calculated instead, the spectrometer could be replaced with a detector which would allow much faster acquisition. Additionally, if each individual element were measured separately rather than the entire sample, then illumination and detection parameters could be tailored to the reflectance conditions of the element. This would increase the amplitude and improve the resolution of the signal, at a cost of an increase in the overall measurement time. To further test the capability of the technique by further reduction the refractive index contrast, the windows could be replaced with elements constructed of lower index materials. For example, calcium fluoride and fused silica have refractive indices (n_p) of 1.4302 and 1.4527 (at 840 nm) respectively. For CaF_2, this is sufficient to match sucrose solution at 60% concentration, and for fused silica the difference is ~0.02. The result of all this could potentially lead to in-situ measurement of the thickness and refractive index of the ocular components of the eye which would inform surgeons of the refractive properties of the intra-ocular lenses that are implanted during cataract surgery, ultimately leading to improved vision post-surgery.

Funding. Engineering and Physical Sciences Research Council (EP/M010473/1, EP/H02252X/1).

Acknowledgment. The authors would like to acknowledge Guy Smith of the Matrix Eye Clinic, Swindon, UK for useful discussions on the eye and ophthalmic instrumentation.

Disclosures. The authors declare that they have no competing interests.

Data availability. The underlying data can be accessed in [30].

Supplemental document. See Supplement 1 for supporting content.

References

1. M. Haruna, M. Ohmi, T. Mitsuyama, *et al.*, "Simultaneous measurement of the phase and group indices and the thickness of transparent plates by low-coherence interferometry," Opt. Lett. **23**(12), 966–968 (1998).
2. S. Kim, J. Na, M. J. Kim, *et al.*, "Simultaneous measurement of refractive index and thickness by combining low-coherence interferometry and confocal optics," Opt. Express **16**(8), 5516–5526 (2008).
3. D. Francis, H. D. Ford, and R. P. Tatam, "Spectrometer-based refractive index and dispersion measurement using low-coherence interferometry with confocal scanning," Opt. Express **26**(3), 3604–3617 (2018).
4. G. J. Tearney, M. E. Brezinsky, J. F. Southern, *et al.*, "Determination of the refractive index of highly scattering human tissue by optical coherence tomography," Opt. Lett. **20**(21), 2258–2260 (1995).
5. E. D. Moore and R. R. McLeod, "Phase-sensitive swept-source interferometry for absolute ranging with application to measurements of group refractive index and thickness," Opt. Express **19**(9), 8117–8126 (2011).
6. J. Na, H. Y. Choi, E. S. Choi, *et al.*, "Self-referenced spectral interferometry for simultaneous measurements of thickness and refractive index," Appl. Opt. **48**(13), 2461–2467 (2009).
7. T. Kim, M. Choi, B. J. Lee, *et al.*, "Liquid refractive index measurements using cavity in silicon via near-infrared interferometry," Sens. Actuators, A **381**, 116078 (2025).
8. J. Yao, J. Huang, P. Meemon, *et al.*, "Simultaneous estimation of thickness and refractive index of layered gradient refractive index optics using a hybrid confocal-scan swept- source optical coherence tomography system," Opt. Express **23**(23), 30149–30164 (2015).
9. Y. Zhang and Q. Zhang, "Simultaneous measurement of thickness and group refractive index in birefringent crystals," Meas. Sci. Technol. **35**(8), 085114 (2024).
10. T. Szarlan, D. Gibson, X. Wei, *et al.*, "Accurate measurements of phase refractive index of soft contact lenses," Opt. Express **28**(8), 10818–10835 (2020).
11. M. T. El-Haddad and Y. K. Tao, "Non-contact characterization of compound optical elements using reflectance confocal microscopy, low-coherence interferometry, and computational ray-tracing," Sci. Rep. **9**(1), 17111 (2019).
12. Z. Wang, Z. Ni, Y. Bai, *et al.*, "Advanced chromatic confocal optical coherence tomography sensor with switchable acquisition modes," Opt. Laser Technol. **182**, 112182 (2025).

Optics EXPRESS

13. D. Mishra, G. Shilpkala, K. Glover, *et al.*, "Vitreous humor: composition, characteristics and implication on intravitreal drug delivery," Curr. Eye Res. **48**(2), 208–218 (2023).
14. L. Tutchenko, S. Patel, O. Horak, *et al.*, "Effect of cataract surgery on the refractive index of the cornea estimated by optical pachymetry," Cornea **37**(11), 1414–1420 (2018).
15. S. Patel and L. Tutchenko, "The refractive index of the human cornea: A review," Cont. Lens Anterior Eye **42**(5), 575–580 (2019).
16. S. R. Uhlhorn, D. Borja, F. Manns, *et al.*, "Refractive index measurement of the isolated crystalline lens using optical coherence tomography," Vision Res. **48**(27), 2732–2738 (2008).
17. D. Huang, E. A. Swanson, C. P. Lin, *et al.*, "Optical coherence tomography," Science **254**(5035), 1178–1181 (1991).
18. D. Francis, J. M. Hallam, and R. P. Tatam, "Low-coherence and broadband confocal refractometry: reducing the measurement time," Meas. Sci. Technol. **34**(12), 125204 (2023).
19. H. D. Ford, D. Francis, J. M. Hallam, *et al.*, "Influence of aberrations on confocal-based remote refractive index measurements," Appl. Opt. **58**(24), 6474–6485 (2019).
20. H. Maruyama, S. Inoue, T. Mitsuyama, *et al.*, "Low-coherence interferometer system for the simultaneous measurement of refractive index and thickness," Appl. Opt. **41**(7), 1315–1322 (2002).
21. P. Liu, R. Groves, and R. Benedictus, "Signal processing in optical coherence tomography for aerospace material characterization," Opt. Eng. **52**(3), 033201 (2013).
22. P. Pavliček and V. Michálek, "White-light interferometry - envelope detection by hilbert transform and influence of noise," Opt. Laser. Eng. **50**(8), 1063–1068 (2012).
23. J. C. Dainty, *Laser speckle and related phenomena* (Springer-Verlag, Berlin Heidelberg, 1975).
24. R. C. Weast, *CRC Handbook of chemistry and physics, 64th edition* (CRC Press, 1984).
25. M. N. Polyanskiy, "Refractiveindex.info database of optical constants," Sci. Data **11**(1), 94 (2024).
26. Schott, "Optical glass data sheets," (2017).
27. M. Daimon and A. Masumura, "Measurement of the refractive index of distilled water from the near-infrared region to the ultraviolet region," Appl. Opt. **46**(18), 3811–3820 (2007).
28. M. Misto, E. Purwandari, Supriyadi, *et al.*, "Analyses of concentration and wavelength dependent refractive index of sugar solution using sellmeier equation," J. Phys.: Conf. Ser. **1825**(1), 012030 (2021).
29. D. A. Atchison and G. Smith, "Chromatic dispersions of the ocular media of human eyes," J. Opt. Soc. Am. A **22**(1), 29–37 (2005).
30. D. Francis, J. Hallam, and R. Tatam, "Data for: Performance of low-coherence and confocal refractometry with reduced index contrast," Cranfield University 2025, https://doi.org/10.57996/cran.ceres-2792.

519.111.36 2026-01-23 03:57:39



https://dspace.org/

The performance of low-coherence and confocal refractometry with reduced index contrast

Francis, Daniel; Hallam, Jonathan M.; Tatam, Ralph P.

2026-01-26
Optica Publishing Group
https://doi.org/10.1364/oe.582088
Francis D, Hallam JM, Tatam RP. (2026) The performance of low-coherence and confocal refractometry with reduced index contrast. Optics Express, Volume 34, Issue 2, January 2026, pp. 2714-2728

Downloaded from a DSpace repository. https://dspace.org/